Journal of Catalysis **204,** 259–271 (2001)
doi:10.1006/jcat.2001.3400, available online at http://www.idealibrary.com on IDEAL®

Structural and Catalytic Properties of Ni/SiO_2 Prepared by Solution Exchange of Wet Silica Gel

Ryoji Takahashi,*,[1] Satoshi Sato,* Toshiaki Sodesawa,* Masayuki Kato,†
Shoichi Takenaka,† and Satoshi Yoshida‡

*Department of Materials Technology, Faculty of Engineering, Chiba University, Yayoi, Inage, Chiba 263-8522, Japan; †Graduate School of Science and Technology, Chiba University, Yayoi, Inage, Chiba 263-8522, Japan; and ‡Department of Materials Science, School of Engineering, University of Shiga Prefecture, 2500 Hassaka, Hikone, Shiga 522-8533, Japan

Received January 22, 2001; revised August 9, 2001; accepted August 15, 2001

Structural formation of Ni/SiO_2 in a solution exchange method, where Ni was supported on silica by exchanging the solution in wet silica gel derived from tetraethoxysilane under acidic conditions, and its catalytic property were investigated. In the preparation of Ni/SiO_2, the dispersion of Ni is largely dominated by aggregation in drying, while mesopore structure in the silica support can be controlled to ∼4 nm by exchanging the solution with strong acids. When aqueous nickel nitrate solution is used in the solution exchange, large nickel nitrate crystals are formed within the gel matrix during drying. They decompose into aggregates of NiO crystallites, with sea–island distribution during calcination. On the other hand, the use of citric acid together with nickel nitrate in the solution exchange effectively inhibits the aggregation of Ni species in drying through the formation of nickel citrate, which barely crystalizes in drying. In calcination, the nickel citrates decompose into NiO particles, and their distribution in the silica matrix becomes homogeneous. Additionally, the use of citric acid and calcination in an inert atmosphere has another effect, decreasing the particle size of NiO and Ni. Consequently, we can prepare Ni/SiO_2 catalyst with high Ni surface area at high Ni content, which shows superior catalytic activity in the hydrogenation of benzene.

Key Words: **silica-supported nickel; solution exchange; sol–gel; hydrogenation of benzene; dispersion control of metal particles.**

INTRODUCTION

Supported nickel catalysts such as Ni/Al_2O_3 and Ni/SiO_2 have been widely used for catalytic reactions, such as hydrogenation, hydrogenolysis, and methane reforming (1–7). In the preparation of catalysts, improvement of dispersion of Ni and precise design of pore structure are particularly important for high catalytic performance. Conventionally, silica-supported Ni catalysts were prepared by ion exchange and impregnation methods. Since the 1980s, a sol–gel method, which was initially introduced as a new method to prepare glasses and ceramics in the 1970s (8), has been attracting much attention as a new process for preparing solid catalysts (9). Because a sol–gel-derived gel, an intermediate for glass formation, has pores with various structures, the sol–gel method is considered to be a promising route for preparation of well-designed porous materials. Furthermore, various composites and compounds can be prepared from a homogeneous solution via nonequilibrium processes. These features of the sol–gel method are suitable for controlling the structure of solid catalysts. Many researchers have reported preparation and characterization of sol–gel-derived catalysts, such as SiO_2–Al_2O_3 (10), SiO_2–ZrO_2 (11, 12), and silica-supported metal catalysts (13–18).

Ni/SiO_2 catalysts have also been prepared using sol–gel processes. For example, Ueno and co-workers prepared Ni/SiO_2 from tetraethoxysilane (TEOS) and nickel nitrate by using ethylene glycol as a solvent and a ligand for Ni (13, 14). Breitscheidel *et al.* used aminoalkyl alkoxysilane as a silica source, expecting coordination bonding between Ni and the amino groups (16). It has been shown that the Ni particles are homogeneously dispersed in the silica gel matrix by adopting the sol–gel method even at higher Ni content, typically up to 30 wt% of Ni. However, the particle size of Ni increases with the increase in the Ni content, and becomes larger than 10 nm when Ni is more than 10 wt%.

If we can keep the small particle size of Ni even at high Ni content, we will improve the catalytic activity by simply increasing Ni loading. A decrease in particle size sometimes has another effect, increasing a specific activity (i.e., turnover frequency (TOF)), or changing product selectivities (13). In addition, pore structure control of silica support is also important in designing the structure of supported metal catalysts. Our goal is to establish a procedure by which a Ni/SiO_2 catalyst with a well-designed pore structure and high Ni dispersion can be prepared. Relating to the pore structure design of silica support, one of the authors has demonstrated that the pore structure of amorphous silica

[1] To whom correspondence should be addressed. Fax: +81-43-290-3376. E-mail: rtaka@tc.chiba-u.ac.jp.

0021-9517/01 $35.00

gel derived from sol–gel processes can be precisely controlled by the solution exchange of wet silica gel (19, 20).

In our latest letter, we reported an application of the solution exchange to the preparation of Ni/SiO_2 where an aqueous nitric acid solution containing nickel nitrate was used in the solution exchange (21). In the process, Ni/SiO_2 prepared in the presence of citric acid in solution exchange showed high Ni surface area and superior catalytic activity for the hydrogenation of benzene. In this work, we investigate the structure formation process of Ni/SiO_2 and clarify the effect of the use of citric acid in solution exchange on high dispersion of Ni. The catalytic activity of the Ni/SiO_2 is also examined in detail.

METHODS

Catalyst Preparation

Nickel nitrate hexahydrate (Wako Chemical Co.) and TEOS (Shin–Etsu Chemical Co.) were used as sources of nickel and silica, respectively, without further purification. Nitric acid (Wako Chemical Co.) was used as a catalyst for hydrolysis and polycondensation of TEOS. Citric acid monohydrate (Wako Chemical Co.) was used as an additive in solution exchange.

The Ni/SiO_2 catalysts were prepared as reported previously (21). A 10 cm^3 amount of TEOS and a 10 cm^3 amount of 1 mol dm^{-3} of nitric acid aqueous solution was mixed under stirring. After the mixture had become homogeneous, it was sealed in a polystyrene container and kept at 50°C for 20 h for gelation. A transparent wet gel monolith was obtained with typical dimensions of ca. $50 \times 60 \times 7$ mm. It was immersed in a 1 mol dm^{-3} nitric acid aqueous solution, with a volume five times as large as the gel volume, at 25°C. The external solution was renewed every 2 h three times. Finally, the wet gel was immersed in a 1 mol dm^{-3} nitric acid aqueous solution containing in appropriate concentration of nickel nitrate for 1 day to exchange the swelling solution to the Ni-containing one (denoted as NA). In some cases, citric acid equimolar with an Ni ion was also dissolved in the exchange solution, where a nickel citrate complex was formed in the solution (denoted as CA).

The obtained wet gel containing the Ni ion or nickel citrate complex was dried at 50°C until no shrinkage was detected. After the dried gel was crushed into powder, it was heated in air at 180°C for 1 h, followed by calcination in air (NA–air and CA–air) or under N_2 (NA–N_2 and CA–N_2) flow at 500°C for 2 h to obtain a NiO/SiO_2 sample. The structural features of the sample in the CA series varied largely with the atmosphere in calcination, whereas NA–N_2 and NA–air samples showed almost the same structural features. Hereafter, NA–N_2 samples are not referred to. The NiO/SiO_2 samples were reduced in an H_2 flow at 500°C for 2 h before the H_2 adsorption measurement and catalytic reaction of benzene with H_2.

For comparison, NiO/SiO_2 samples were also prepared by the usual impregnation method (denoted as IMP) and the sol–gel method using ethylene glycol as a solvent [14] (denoted as EG).

The Ni content in each Ni/SiO_2 was determined from both the weight increase against the reference sample without Ni and H_2 consumption during temperature-programmed reduction (TPR) measurement. Experimental errors in the values obtained by the weight and the TPR methods were less than 1%. The Ni content in the catalyst was denoted as mole percent of Ni, $100 \times [Ni_{mol}]/([Ni_{mol}] + [Si_{mol}])$, and was controlled by altering the concentration of nickel nitrate solution for the sample prepared by solution exchange.

Characterization of Catalysts

^{29}Si magic angle spinning (MAS) nuclear magnetic resonance (NMR) spectra were recorded on a DPX300 spectrometer (Bruker) with pulse sequences of high-power decoupling for the reference silica gel samples without nickel. Details of the measurement conditions are described elsewhere (22). Small-angle X-ray scattering (SAXS) measurement for the nickel-less sample was performed on a RINT system (Rigaku). Details of the apparatus, measurement conditions, and data processing were described previously (23).

TPR measurements were carried out from 50 to 900°C in a conventional apparatus with a thermal conductivity detector (TCD) under the following conditions: heating rate, 5 K min^{-1}; flow rate of nitrogen gas containing 10% hydrogen, 10 cm^3 min^{-1}; sample weight, 10.0 mg. The Ni content in the sample was calculated by integrating the reduction peaks. X-ray diffraction (XRD) patterns were recorded on a M18XHF (MAC Science) using Cu$K\alpha$ radiation ($\lambda =$ 0.154 nm). A transmission electron microscope (TEM; H-8100, Hitachi) was used for some samples. The accelerating voltage was 200 kV.

Nitrogen adsorption–desorption isotherms for NiO/SiO_2 samples at −196°C were measured using Omnisorp 100CX (Coulter). Each sample was degassed at 300°C for 1 h under vacuum before each measurement. The specific surface area was calculated from the adsorption curve according to the BET method. The pore-size distribution was calculated from both the adsorption and the desorption curves by the Dollimore–Heal method (24). Measurement of H_2 chemisorption was performed with a volumetric apparatus at 0°C to calculate nickel metal surface area of the reduced sample. Prior to the measurement, the sample was re-reduced by repeated exposure to 200 mm Hg H_2 at 500°C, and then outgassed under vacuum for 1 h at the same temperature to remove H_2 adsorbed on the sample. The isotherm was fitted to a Langmuir equation to obtain a monolayer-adsorption amount, and then the Ni metal surface area was calculated from the adsorbed H_2 amount, assuming that chemisorption stoichiometry is H/Ni = 1

and that a Ni atom occupies 0.065 nm^2 on a Ni particle (25, 26).

Catalytic Reaction

The hydrogenation of benzene was performed in a conventional fixed-bed flow reactor under atmospheric pressure of H_2 at a temperature range between 80 and 280°C. Prior to the reaction, a NiO/SiO_2 sample with a weight of 0.05–0.3 g was reduced under H_2 flow at 500°C for 2 h. In the reaction, benzene was fed into the reactor with a flow rate of 14.3 mmol h^{-1} together with an H_2 flow of 119 mmol h^{-1}. The reaction products were analyzed with on-line TCD–gaschromatography with a packed column of squalane (2 m) at 40°C. A space–time yield at 80°C was obtained by changing the catalyst weight to control the conversion level at ~10%.

RESULTS

Structural Characteristics of NiO/SiO_2 and Ni/SiO_2 Prepared by Solution Exchange

Table 1 summarizes the structural properties of NiO/SiO_2 samples and their reduced bodies, and Fig. 1 shows pore-size distribution curves of the samples. Generally, hysteresis behavior in N_2 isotherms, which are frequently observed in amorphous silicas, have been ascribed to the presence of ink–bottle-shaped pores (27). Then, pore-size distribution calculated from an adsorption branch (broken line) contains information on the maximum size of pores in which metal particles can grow without breaking pore structure of silica gel, while that calculated from a desorption branch (solid line) is a measure of the neck size of pores at which molecular transportation is mostly restricted. For all the samples, the pore-size distribution by the adsorption branch is broader than that by the desorption one. Here after, we mainly refer to the pore-size distribution curves from desorption branches, because it is convenient for comparison with the literatures. A silica gel without Ni (NA-0) has mesopores with a peak in pore-size distribution at 4 nm, a BET surface area of 650 m^2 g^{-1}, and mesopore volume of 0.50 cm^3 g^{-1}. These values agree well with those reported previously for a gel prepared by solution exchange with a 1 mol dm^{-3} nitric acid aqueous solution (19). In the NA–air series, the average pore size increases with an increase in Ni content (Fig. 1a), while the mesopore volume barely changes. As a result, BET surface area decreases with an increase in Ni content. In contrast, a small change in pore structure is observed in the CA series (Fig. 1b). Although BET surface area and pore volume decrease with increasing Ni for the CA series, the values based on the silica weight

TABLE 1

Structural Properties of NiO/SiO_2 and Ni/SiO_2 Samples

	NiO/SiO_2					Ni/SiO_2		
Catalyst[a]	NiO (wt%)	BET SA[b] (m^2 g^{-1})	PV[c] (cm^3 g^{-1})	PS[d] (nm)	NiO CS[e] (nm)	$Ni_{surface}$ [f] (mmol g^{-1})	Ni SA[b] (m^2 g^{-1})	D[g] (%)
NA-0	0	650	0.50	3.1	—	—	—	—
NA–air-8	10	618	0.51	3.3	8.4	0.092	3.6	6.8
NA–air-15	18	560	0.53	3.8	9.6	0.170	6.7	7.1
NA–air-19	23	235	0.34	5.8	9.4	0.266	10.4	8.6
NA–air-26	30	220	0.49	8.9	9.8	0.316	12.3	7.9
CA–air-8	10	401	0.62	6.2	6.5	0.078	3.1	5.9
CA–air-15	18	390	0.72	7.4	6.3	0.248	9.7	10.3
CA–air-19	23	428	0.52	4.9	6.8	0.278	10.9	9.0
CA–air-26	30	342	0.42	4.9	6.7	0.376	14.7	9.3
CA–N_2-8	10	483	0.67	5.5	3.4	0.176	6.9	13.1
CA–N_2-15	18	495	0.64	5.2	3.5	0.328	12.8	13.6
CA–N_2-19	23	300	0.50	6.7	3.4	0.560	21.9	17.1
CA–N_2-26	30	418	0.51	4.9	3.6	0.684	26.7	17.0
EG-8	10	198	0.23	4.6	10.8	0.116	4.6	8.7
EG-26	30	219	0.20	3.7	6.0	0.234	9.1	5.8
IMP-8[h]	10	—	—	—	13.0	0.124	4.9	9.3
IMP-26[h]	30	—	—	—	12.0	0.204	8.0	5.0

[a] The number indicates Ni content in mol%.
[b] SA, surface area.
[c] PV, total pore volume. Obtained from N_2 adsorption volume at $P/P_0 > 0.95$.
[d] PS, average pore size. Obtained from 4 × SA/PV.
[e] CS, crystallite size. Estimated from XRD peak width at 62.8° according to Scherrer's equation.
[f] Number of surface Ni atom calculated from monolayer adsorption amount of H_2.
[g] Dispersion obtained by 100 × [$Ni_{surface}$]/[Ni_{total}].
[h] NA-0 sample was used as the silica support.

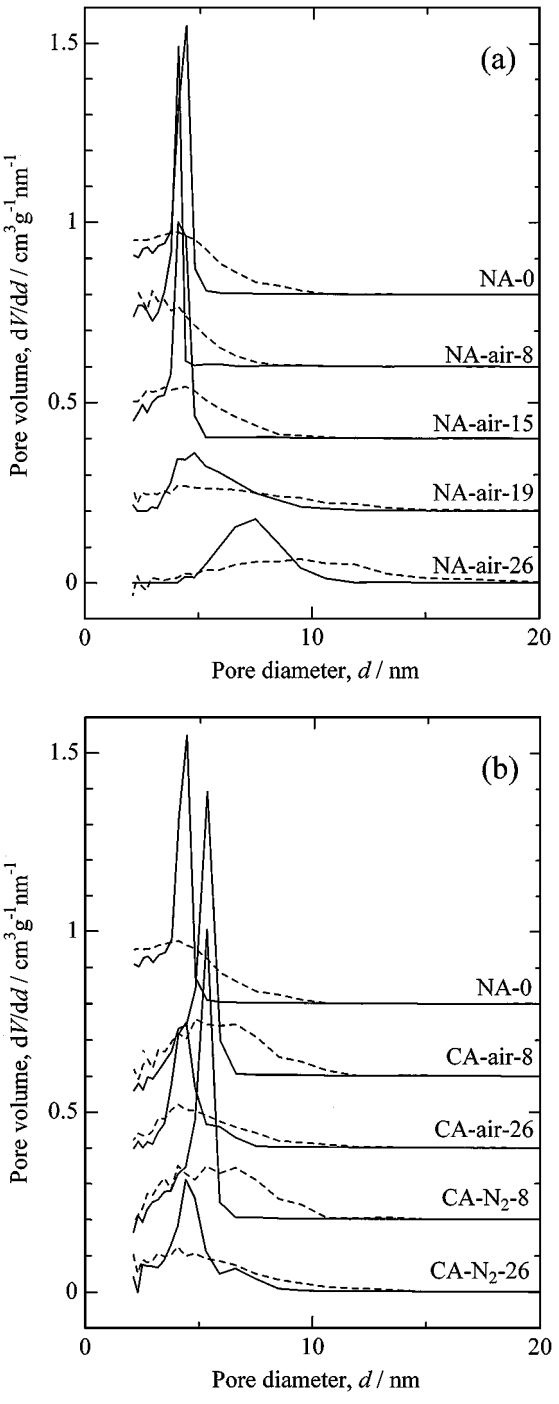

FIG. 1. Pore size distributions of NiO/SiO_2 samples for (a) NA and (b) CA series. Characters on the profiles correspond to catalyst denotation listed in Table 1. Solid lines are calculated from desorption curves, and broken ones are from adsorption curves.

remain almost constant. The EG samples show BET surface area and pore volume smaller than those of the NA and CA series.

Figure 2 shows XRD profiles of NiO/SiO_2 samples prepared using different methods. All the profiles except that of the $CA–N_2$ sample consist of a hollow of amorphous silica and three peaks ascribed to diffraction from cubic NiO crystals. The $CA–N_2$ sample contains metal Ni in addition to silica and NiO. In the sample, citric acid probably acts as a reducing reagent under heating in the inert atmosphere. The full width at a half maxima (FWHM) of diffraction peaks of NiO varies among the samples. A crystallite size estimated from the FWHM according to Scherrer's equation is summarized in Table 1. The crystallite size slightly changes against the change in Ni content, while it strongly depends on the preparation route. Some researchers reported the increase in particle size of Ni or NiO with increasing the Ni content not only in conventional methods but also in sol–gel routes (13, 16). Therefore, the fact that one can control NiO particle size irrespective of Ni content by adopting the solution exchange is interesting. In the solution exchange, furthermore, the particle size of NiO can be decreased from ~9 nm to ~6.5 nm by adding citric acid. In addition, the calcination of CA samples under N_2 flow has the drastic effect of decreasing particle size; the particle size of NiO in all the $CA–N_2$ samples is as small as ~3.5 nm.

Figure 3 shows XRD profiles of reduced bodies of the samples shown in Fig. 2. Even after reduction at 500°C, NiO remains in the CA–air and EG samples. The Ni crystallite sizes estimated from FWHM of the diffraction peaks of Ni crystal in reduced samples are somewhat smaller than those of NiO in calcined samples. The result suggests that aggregation of Ni in reduction barely proceeds in all the

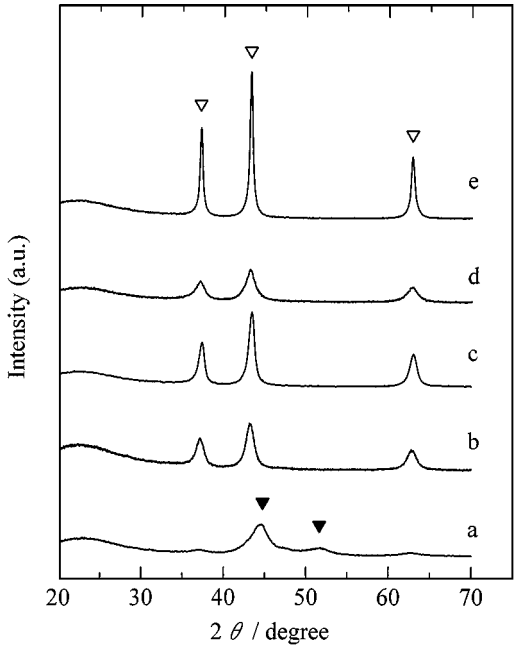

FIG. 2. XRD patterns of the samples calcined at 500°C. (a) $CA–N_2$-26, (b) CA–air-26, (c) NA–air-26, (d) EG-26, and (e) IMP-26. Peaks with open triangles are from NiO crystal and those with closed triangles are from Ni crystal.

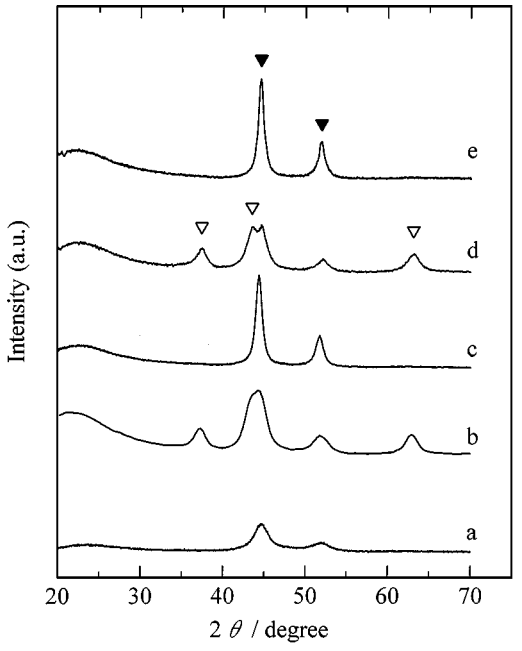

FIG. 3. XRD patterns of the samples reduced with H_2 at 500°C. (a) CA–N_2-26, (b) CA–air-26, (c) NA–air-26, (d) EG-26, and (e) IMP-26. Peaks with open triangles are from NiO crystal and those with closed triangles are from Ni crystal.

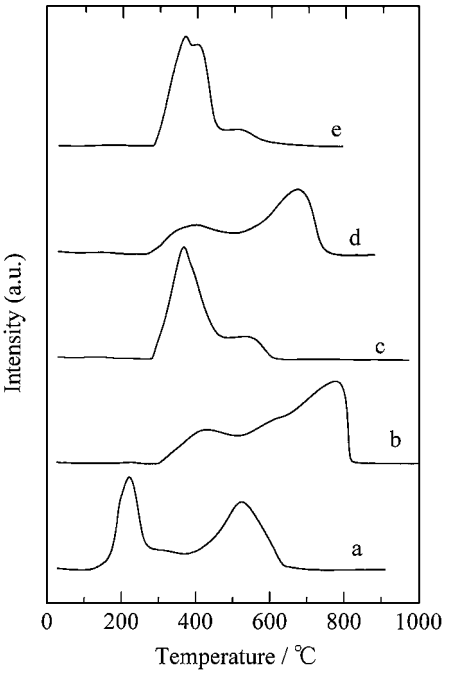

FIG. 4. TPR profiles of the calcined samples. (a) CA–N_2-26, (b) CA–air-26, (c) NA–air-26, (d) EG-26, and (e) IMP-26.

samples. Consequently, it can be realized that the Ni surface area measured by H_2 chemisorption increases with an increase in Ni content in each series of samples, and that it increases with a decrease in NiO particle size in unreduced samples at a constant Ni content (Table 1).

Figure 4 shows TPR profiles of NiO/SiO_2 samples. In TPR profiles, nickel oxides isolated in the bulk and those attached to silica have been reported to be reduced at 300–400 and 400–500°C, respectively (28). In the IMP sample, most of nickel oxides are in the bulk, and a small amount is attached to silica. The NA–air sample shows a profile similar to the IMP sample. On the other hand, EG and CA–air samples are reduced at higher temperatures, over 600°C. In the CA–N_2 sample, about half of the NiO is easily reduced at as low as 200°C. Thus, the difference in calcination conditions affects not only the particle size of NiO but also the reducibility of the NiO species.

Figure 5 shows a TEM micrograph of CA–air-26 reduced at 500°C. Particles with sizes ranging from ca. 2 to 10 nm randomly disperse in silica matrix. In some particles, lattice fringe images can be recognized (indicated by arrows). The lattice spacing, 0.20 nm, agrees well with plane distance of (111) plane in the cubic Ni crystal. Then, each particle observed in the TEM can be regarded as a single crystallite without coagulation. Figure 6 shows TEM micrographs with low magnification. Clearly, distribution of Ni particles in the silica matrix is homogeneous in the reduced CA–air-26 (Fig. 6A) and CA–N_2-26 (Fig. 6C) samples, whereas the particle size is larger in the CA–air-26 sample. Homogeneous

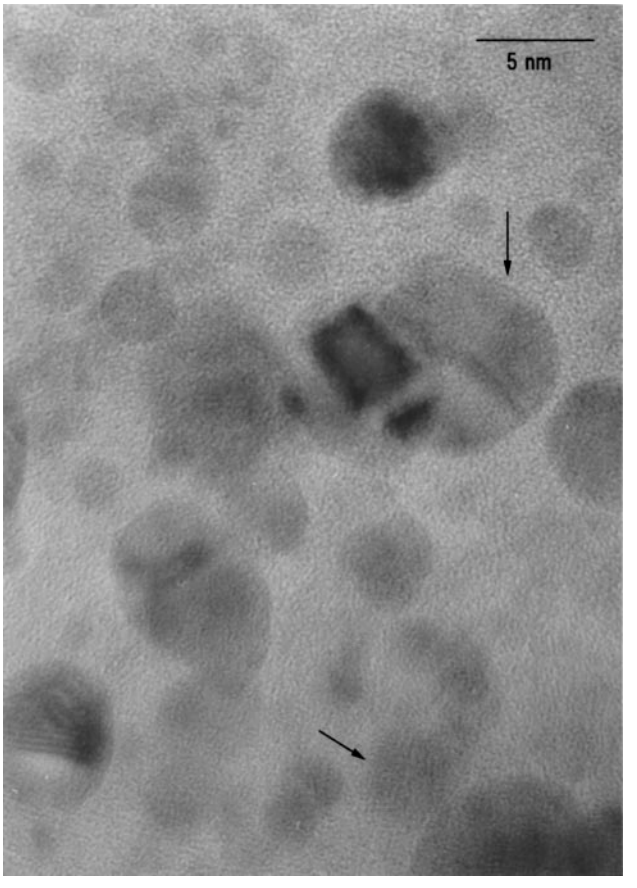

FIG. 5. TEM photograph of the reduced CA–air-26 sample. The arrows indicate particles with lattice fringe images.

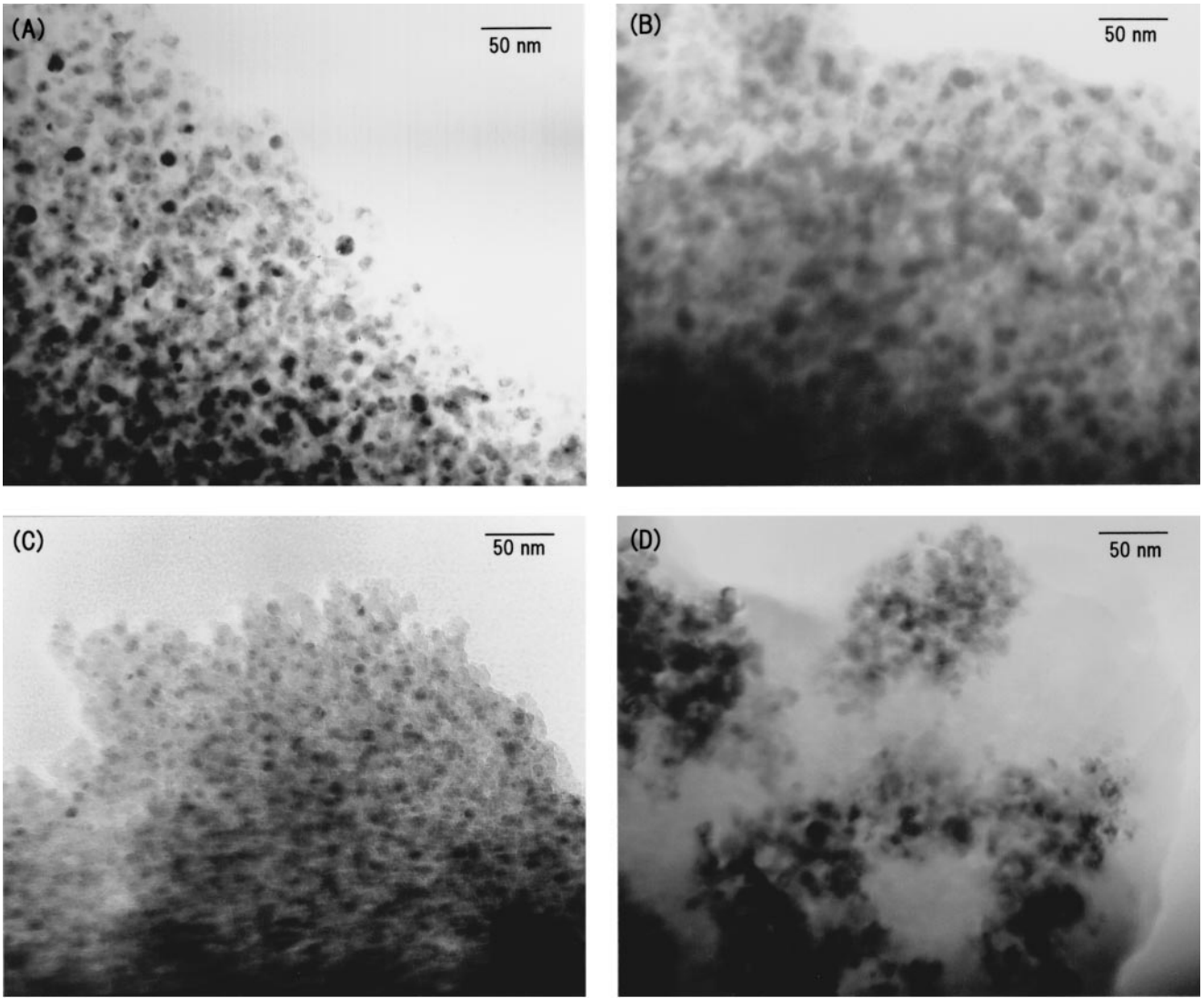

FIG. 6. TEM photographs of (A) reduced CA–air-26, (B) calcined CA–air-26, (C) reduced CA–N_2-26, and (D) reduced NA–air-26 samples.

dispersion of NiO particles is also detected in the CA–air-26 sample before reduction (Fig. 6B). On the other hand, characteristic assembly of Ni particles is observed in the NA–air-26 sample (Fig. 6D). In the sample, several tens of Ni particles gather, forming aggregates, and a typical sea–island structure is formed. It seems that no contact occurs among particles in the aggregates. This type of sea–island structure is also observed in the NA–air sample with low Ni content (8 mol%) (29). Therefore, the formation of the sea–island structure is considered to be a characteristic feature in the NA–series samples.

Observation of Structural Evolution during Processing

Figure 7 shows a change in the XRD profiles in calcination for the NA–air-26 sample. Sharp diffraction peaks corresponding to nickel nitrate are observed in samples dried at 50°C (Fig. 7b). On heating, the nickel nitrate decomposes, and NiO crystals appear over 250°C. The diffraction peaks of NiO are much broader than those of nickel nitrate, suggesting large nickel nitrate crystals decompose into a large number of small NiO particles in heating. Here, it must be noted that no diffraction corresponding to nickel nitrate is observed in the CA sample dried at 50°C (Fig. 7a). These differences in the structure formation behavior will result in the differences in microstructures among the samples, as observed with TEM.

To clarify the structural formation of silica support, ^{29}Si MAS–NMR and SAXS measurements were performed for reference NA-0 samples. Figure 8 shows changes in ^{29}Si MAS–NMR spectra in sol–gel processing for the pure silica gel without Ni (NA-0). The peaks at ca. −90, −100,

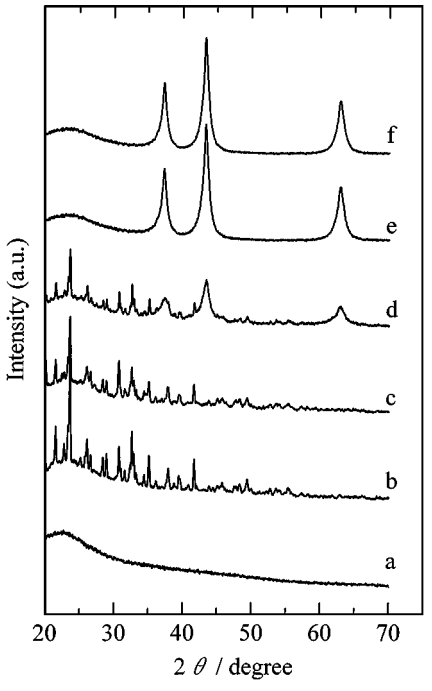

FIG. 7. Variations in XRD profiles with different heating temperatures. (a) CA-26 dried at 50°C, (b) NA-26 dried at 50°C, and heated in air at (c) 200°C, (d) 250°C, (e) 300°C, and (f) 500°C.

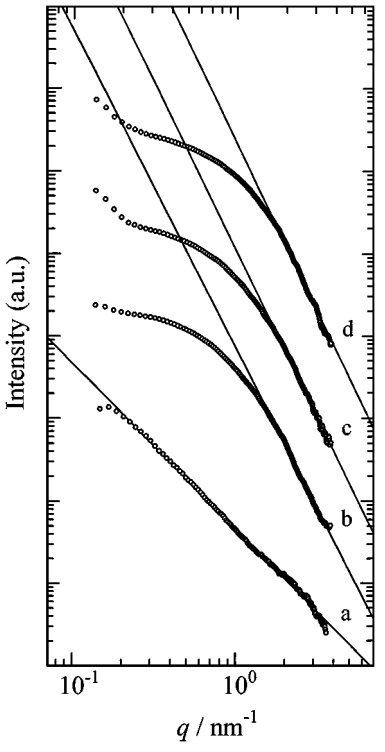

FIG. 9. SAXS profiles for NA-0 samples. The intensity is arbitrarily shifted for clarity. (a) Wet gel, (b) gel dried at 50°C, (c) heated at 300°C, and (d) heated at 500°C. Slopes of the fitting lines in power law are −2.0, −3.8, −4.0, and −4.1 from the bottom line in turn.

and −110 ppm have been ascribed to Q^2, Q^3, and Q^4 silicons, respectively (8). Here, Q^n indicates a formula of $Si(OSi)_n(OR)_{4-n}$, where R is an alkyl group or a hydrogen. In the wet state (Fig. 8a), the gel consists of mainly Q^3 and Q^4. The large amount of Q^3 and the narrow width of each peak suggests that condensation of silica species in the gel does not so proceed. The Q^3 peak becomes smaller and each peak becomes broader during drying and heating (Figs. 8b and 8c). Finally, only a shoulder is observed at the chemical shift of Q^3 in the sample heated at 500°C (Fig. 8d).

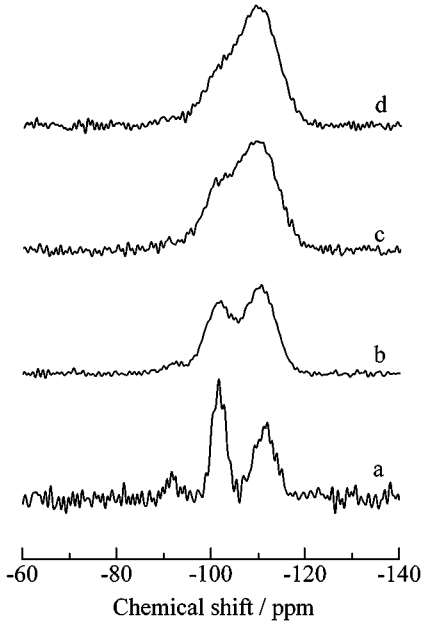

FIG. 8. ^{29}Si MAS–NMR spectra for NA-0 samples. (a) Wet gel, (b) gel dried at 50°C, (c) heated at 300°C, and (d) heated at 500°C.

Figure 9 shows changes in the SAXS profiles in sol–gel processing for the NA-0 sample. Here, the scattering wavenumber vector, q, represented with scattering angle by $q = (4\pi/\lambda)\sin(\theta)$, is related to structural size in a real space, l, by $l = 2\pi/q$. We can obtain information on a mesoscale structure with SAXS measurements in contrast to the NMR, which shows structural information on the atomic scale. According to the literatures, the slope in a $\log(I)$–$\log(q)$ plot can be related to the fractal dimension of the scattering objects if a linear portion presents (8). When the slope, s, is −4, the scattering object has no more fractal nature. At $-4 < s < -3$, the slope is related to the surface fractal dimension by $d_s = 6 - s$. At $s > -3$, the slope is related to the mass fractal dimension by $d_m = -s$. Among the profiles, the feature of the profile of the wet gel (Fig. 9a) is clearly different from other profiles. The scattering intensity monotonically decreases with scattering vector, and the slope is −2. This suggests that the scattering objects in the wet gel have a fractal nature, with a mass fractal dimension of 2. That is, the wet silica gel formed in the acidic conditions can be regarded as a polymeric network rather than particle aggregates. On drying at 50°C, the scattering profile

drastically changes (Fig. 9b). An upward convex dependence is observed in the dried samples, and the slope at higher q range is nearly -4. This upward convex curve could be interpreted as combined power-law slope indicative of the presence of dense particles with smooth surfaces building up ramified aggregates (19, 20). Thus, the SAXS results suggest that structural rearrangement on the mesoscale occurs in drying from polymeric network to particle aggregates. Here, the size of a structural unit in the sample dried at 50°C is estimated to be ~5 nm from the scattering vector at the onset of the power-law relation. Structural change on the mesoscale barely proceeds in heating (Figs. 9c and 9d). Then, the increase in the condensation degree of Si shown in ^{29}Si NMR spectra in calcination (Figs. 8b–8d) is attributable to the intraparticle condensation and/or elimination of surface silanols by dehydration, which does not contribute to the change in mesoscale structure.

For the samples containing Ni, ^{29}Si NMR spectra cannot be measured because of the presence of unpaired electrons in Ni^{2+}. Also, it was impossible to interpret SAXS profiles for the samples containing Ni, because the samples are composed of three components with different electron density, silica, nickel species and air, for which no general interpretation method has been proposed.

Hydrogenation of Benzene over Ni/SiO_2 Catalyst

Figure 10 shows changes in conversion of benzene with reaction temperature in the hydrogenation over Ni/SiO_2 catalysts. No catalytic decay was observed at every reaction temperature. Only cyclohexane is detected as a reaction product. Over the catalysts, the conversion of benzene increases with increasing temperature up to ~200°C and then decreases along the equilibrium conversion line. Over the CA–N_2-26 catalyst, the conversion reaches 100% between 120 and 220°C. Here, it must be noted that the monitored reaction temperature is the temperature near the catalyst bed. Because the hydrogenation of benzene is exothermic, the real temperature of the catalyst surface will be somewhat higher than the reaction temperature monitored.

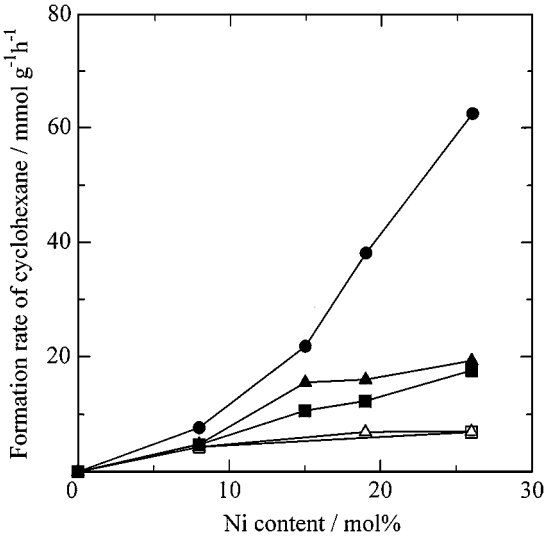

FIG. 11. Variations in the formation rate of cyclohexane at 80°C with Ni content for each series. ●, CA–N_2; ▲, CA–air; ■, NA–air; △, IMP; and □, EG.

Figure 11 shows the formation rate of cyclohexane over various catalysts at 80°C. The formation rate increases with increasing Ni loading for the catalysts prepared by solution exchange. However, the values for reference catalysts saturate over ca. 10–20 mol%. Figure 12 summarizes the

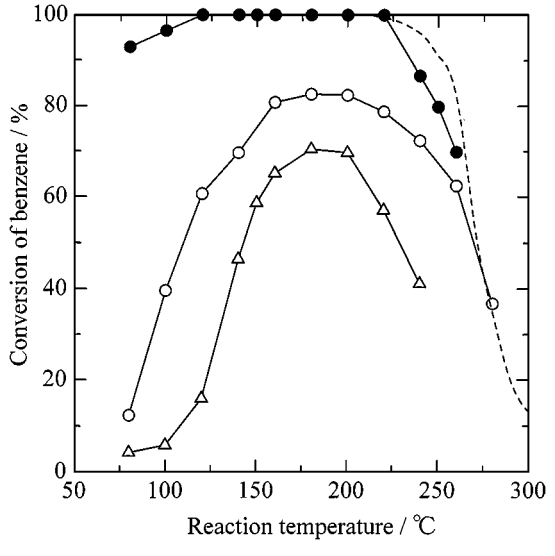

FIG. 10. Variations in conversion of benzene with different reaction temperatures for (●) CA–N_2-26, (○) NA–air-26, and (△) NA–air-8. The broken line indicates the equilibrium conversion.

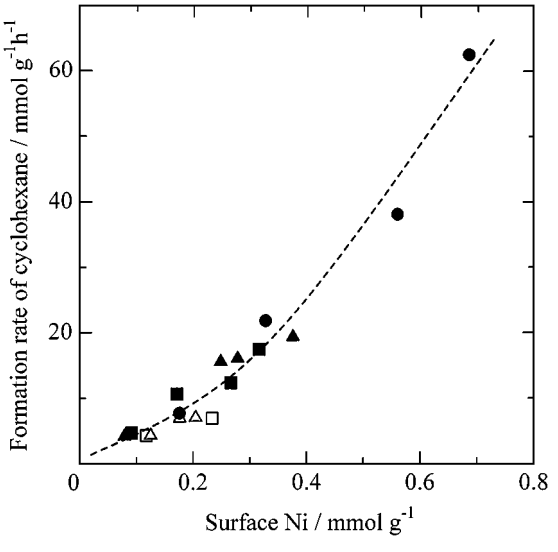

FIG. 12. Dependence of the formation rate of cyclohexane on the amount of surface Ni on each sample. The symbols are the same as those in Fig. 11.

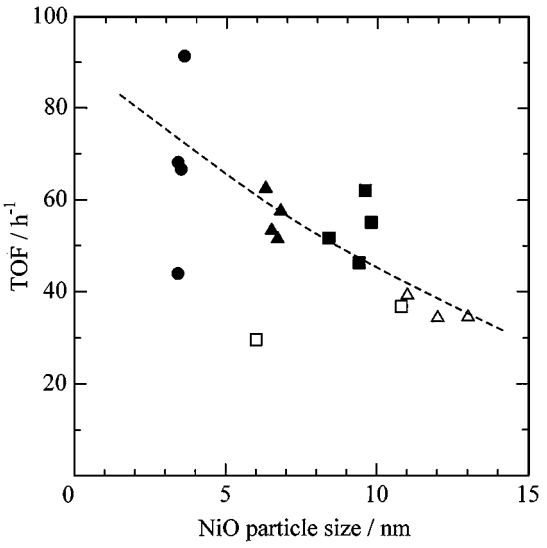

FIG. 13. Relation between TOF in the hydrogenation of benzene and NiO particle size in the unreduced samples. The symbols are the same as those in Fig. 11.

relation between formation rate of cyclohexane and the amount of surface Ni atom. The catalytic activity increases with an increase in the amount of surface Ni. However, the relation between the formation rate and the amount of surface Ni does not seem linear. Then, TOF values obtained by dividing the formation rate by surface Ni are plotted against NiO particle size in an unreduced body in Figure 13. The NiO particle size can be regarded as Ni particle size because aggregation barely proceeds during reduction. It is clear that the TOF increases with decreasing Ni particle size, although some data points deviate largely from the relation.

DISCUSSION

Sol–Gel Preparation of Ni/SiO_2

In the sol–gel preparation of Ni/SiO_2, it has been considered that the bond formation between hetero atoms such as Si–O–Ni is important for high dispersion of Ni (13–16). In the pioneering report by Ueno *et al.*, where ethylene glycol was used as a solvent, they found that the formation of nickel glycoxide occurred in the processing and considered that the reaction between the nickel glycoxide and TEOS leads to the formation of Si–O–Ni bonding (13). Then, Ni is homogeneously entrapped in silica framework on the atomic level, leading to homogeneous distribution of NiO and Ni particles in silica gel matrix after drying, calcination, and reduction. Since then, this concept has been widely accepted in sol–gel preparation of catalysts (16), whereas the Ni particles grow as large as 10 nm in the Ni/SiO_2 at high Ni content.

On the other hand, the incorporation of Ni cations in silica on the atomic scale has been achieved by a deposition–precipitation (DP) method, where the Si–O–Ni bonding is formed by thermal decomposition of urea to increase the solution pH after impregnation (30, 31). A catalyst prepared by the DP method does not show diffraction peaks ascribed to NiO and is formed with amorphous silica, which homogeneously contains Ni cation, and/or with nickel phyllosilicates (30). The NiO/SiO_2 prepared by the DP method shows difficult reducibility. If we consider that the Si–O–Ni bonds are also formed in the sol–gel reaction and are maintained after drying and calcination, we cannot explain why the structure of NiO/SiO_2 prepared in the earlier works of the sol–gel method (13, 16) differs largely from that of the DP method.

In this work, we added the Ni species in silica gel by the solution exchange method instead of direct incorporation in the sol–gel reaction of silica, as adopted by other researchers. The solution exchange possesses an advantage compared with the conventional impregnation: we can support large amount of metals on silica without aggregation at inter grains of silica support because the porosity of the wet silica gel is substantially high. It possesses another advantage compared with the general sol–gel method: we can control the pore structure of silica and dispersion of Ni irrespective of gel preparation conditions. In the process, it is barely considered that a Ni cation is entrapped in the silica framework in the wet gel by the formation of Si–O–Ni bonds because a Ni cation is introduced after the gelation of silica. Actually, the Ni cations introduced in the wet silica gel can be easily extracted by simple immersion of the gel in a water bath (32). Therefore, it is reasonable that the NiO and Ni particle sizes in the present samples are determined by parameters other than the formation of Si–O–Ni bonding.

The average particle size of NiO as well as Ni in the resultant NiO/SiO_2 and Ni/SiO_2 does not exceed 10 nm even for NA series, although the characteristic sea–island structure in distributions of Ni particles is observed (Table 1, Fig. 6D). In addition, the particle sizes of NiO are 6.5 and 3.5 nm for CA–air and CA–N_2 samples, respectively. The addition of citric acid leads to the formation of a stable nickel citrate complex, which barely interacts with the silica gel. These results indicate that Si–O–Ni bond formation during sol–gel reactions of TEOS and Ni cations is not necessary for high dispersion of Ni. In other words, the solution exchange method would be a model case for considering the key role to increase the Ni dispersion in sol–gel-derived Ni/SiO_2.

In the following sections, therefore, we consider how NiO particle size is determined. First, we clarify the nature of the silica gel formed in the present sol–gel process, and how the structure of it develops during processing based on the ^{29}Si MAS–NMR and SAXS results. Then, we consider what parameters affect Ni particle size. Finally, the catalytic characters of the present catalysts for hydrogenation of benzene are discussed.

General Trends of Sol–Gel Reaction under Basic and Acidic Conditions

In a sol–gel preparation of silica from silicon alkoxides, $Si(OR)_4$ where R is an alkyl group, either acid or base, has been widely used as a catalyst for hydrolysis and polycondensation (8). Generally, only a microporous silica gel is obtained under acidic conditions, while a mesoporous silica gel with typical pore size of ~10 nm is formed under basic conditions. This difference in pore structure of the obtained gels has been explained from the reaction mechanism of silica polymer under the respective conditions (8). Since the isoelectric point of silica is ~2, the reactions are catalyzed by OH^- and H^+ at pH >2 and <2, respectively. At pH >2, the hydrolysis and polycondensation of TEOS are promoted by OH^- attaching to Si. Then, an intermediate or transition state with a negative charge is formed. The negative charge on Si is stabilized by surrounding −OSi groups rather than −OH and −OR groups because of an inductive effect. Therefore, the reactions under the basic conditions preferentially occur with condensed species. Furthermore, reverse reactions such as hydrolysis of Si−O−Si bonds are also promoted by OH^-. Thus, a silica gel with a structure like colloidal aggregates is formed. After drying and heating, silica with pore structures reflecting such aggregation structures of colloidal particles are obtained. However, it is difficult to prepare well-designed Ni/SiO_2 catalysts under the basic conditions because heterogeneous precipitation of nickel hydroxide preferentially occurs before gelation of silica.

In contrast, a ramified polymeric network is formed in the wet gel catalyzed by acid. A fractal dimension of 2 for acid-catalyzed wet silica gel estimated from a SAXS profile (Fig. 9a) has been reported by several research groups (23, 33, 34). In addition to the ^{29}Si MAS–NMR results showing that the wet gel is mainly composed of Q^3 and Q^4 silicon (Fig. 8a), the SAXS result suggests that structure of the wet silica gel formed in the present work is far different from stable structures, such as particle aggregates, formed under basic conditions. H^+ attaching to an oxygen in SiOH at pH <2 produces an intermediate or transition state with a positive charge. Then, the reaction under the acidic conditions preferentially occurs at a monomer or end group of weakly branched oligomers because the electron providing ability in the OR and OH groups is higher than that in the OSi group. Thus, an unstable polymeric network with less-branched silica is formed via kinetically controlled reactions. The network structure in the wet silica gel homogeneously shrinks with conversion into microporous silica during drying and heating.

Structural Feature of Silica Gel Prepared by Solution Exchange with Strong Acids

Recently, it was found that the silica gel prepared under acidic conditions shows a feature like organic polymer gels (8). In organic gel systems, reversible swelling and shrinkage of wet gel are frequently observed by changing the pH, temperature, and solvent. This phenomenon is consistently explained as phase transition of the gel network (35, 36). The gel squeezes the solvent out when a repulsive interaction arises between the solvent and the gel network because chemical bonds forming the gel network inhibit the usual phase separation observed in a binary solution system. In some cases, instead of bulk shrinkage the gel turns from clear to opaque due to microscopic-phase separation. The microscopic-phase separation occurs in the gel with high crosslink density (19, 20).

Because of the high coordination number of metal, it had been considered that the inorganic gels were composed of particle aggregates, and the phase transformation observed in organic gels had not been considered to occur in inorganic gels (37). Recently, however, examples of volumetric changes in monolithic wet gel or microscopic-phase separation have been shown by several researchers for inorganic gels. For example, Quinson *et al.* observed volumetric changes in a wet titania gel by changing the swelling solution, where organic reagents were added to decrease the available Ti−O−Ti bonding numbers of titanium (38, 39).

Immersion of a silica gel prepared from TEOS under acidic conditions in an aqueous 1 mol dm^{-3} nitric acid solution also induces microscopic-phase separation on a nanometer scale, leading to density fluctuation (19, 20, 40–43). The size of the density fluctuation is restricted to the correlation length of the wet silica gel, which is typically ~10 nm. In drying, polycondensation in the domains formed by microscopic-phase separation preferentially proceeds to be distinct particles together with bulk shrinkage. As a result, the ramified network in the wet gel converts to particle aggregates in dried gels, as shown in the evolutions of SAXS profiles (Figs. 9a and 9b). In other words, the microscopic-phase separation, which occurs in the wet gel prepared from TEOS under the acidic conditions, can be used in the pore-size control of resultant silica gel (19, 20).

From the view point of the rigidity of the silica gel, the wet silica gel can vary, depending on postgelation treatments, such as aging and solution exchange, due to its fractal nature. On the other hand, the little change in the SAXS profile during calcination (Figs. 9b–9d) indicates that the nanometer-scale structure of the silica gel is fixed after drying.

Structure Formation of SiO_2 in the Presence of Nickel Salts

In the aqueous 1 mol dm^{-3} nitric acid solution, the pore formation of wet silica gel proceeds by physical interaction between silica and solvent. The microscopic-phase separation of the silica gel network and solvent proceeds when the solvent polarity increases substantially. Therefore, it is expected that the addition of metal salt to the

aqueous 1 mol dm^{-3} nitric acid solution has little effect on the phase-separation tendency of the silica network if the additive does not show a special interaction with the silica gel network. Under the present strong acidic conditions, we can ignore the interaction between the silica network and nickel cation because of the high stability in the coordination structure of both the aqua complex of nickel cations and the nickel citrate complex. The results in Fig. 1b showed that the pore structure of the CA-series samples did not change largely: the peak in pore-size distribution was located at 4–6 nm in all the samples. The result suggests that the structural formation of silica by microscopic-phase separation is not affected by the presence of nickel citrate in the acidic solution. On the other hand, the pore size in the NA-series samples increased continuously with an increase in Ni content. At the same time, specific surface area also decreases with an increase in Ni content in the NA series. These structural changes probably occur due to the formation of large nickel nitrate crystals in drying (Fig. 7b). However, the absence of micropores suggests that the pore formation in NA series also proceeds via microscopic-phase separation.

Effect of the Addition of Citric Acid on NiO Dispersion

A characteristic assembly of Ni and NiO particles (i.e., the sea–island structure) is observed in the NA-series samples irrespective of Ni content (Fig. 6D). In a wet silica gel, nickel nitrate crystals grow to a large size in drying, as shown in the XRD profile (Fig. 7b). During calcination, these crystals decompose into small nickel oxide crystallites. The nickel nitrate crystal ($d = 2.50$ g cm^{-3}, $M_r = 290.8$) takes about a 10 times larger molar volume than does the nickel oxide crystal ($d = 6.96$ g cm^{-3}, $M_r = 74.7$). Then, the nickel nitrate crystal fragments into small NiO crystallites with the progress of the decomposition of the nickel nitrate. Therefore, the NiO particles seem to gather in the TEM image (Fig. 6D). That is, each aggregate of nickel oxide crystallite in the calcined samples corresponds to the nickel nitrate crystal in the dried ones. Here, the formation of crystals of nickel nitrate can occur in the wet silica gel because an acid-catalyzed silica gel is formed with a fragile polymeric network and allows fast transportation of nickel and nitrate ions in the gel (29).

Thus, the wet gel with the fractal nature allows aggregation of the nickel species during drying to a large size. It would be a cause of the increase in pore size for NA–air samples (Fig. 1a). In the dried gel, on the other hand, growth of nickel oxide would be restricted to the pore wall of silica, because the pore structure of silica is fixed before calcination, as shown in the SAXS results (Fig. 9). In other words, we can expect a decrease in NiO particle size if the aggregation of Ni species during drying can be restricted.

The use of citric acid in the solution exchange with nickel nitrate has a drastic effect on the dispersion of NiO and Ni in the silica matrix. In contrast to the NA-series samples, which show the characteristic sea–island structure of NiO and Ni particles, homogeneous dispersion of NiO and Ni metal particles is observed in CA-series samples (Fig. 6). In addition, the addition of citric acid decreases the NiO and Ni crystallites sizes (Table 1). Therefore, we can speculate that the aggregation of Ni species during drying is effectively suppressed by the use of citric acid.

Recently, we applied the amorphous citrate process (44–47) to the preparation of catalysts, such as Ni–MgO (26, 48, 49), Cu–MgO (50), $CuAl_2O_4$ (51), and a CeO_2-based solid solution with a fluorite structure (52–54). Various metal cations can form a stable complex with citrate anion in an aqueous solution (55). These metal citrate complexes barely crystalize on drying, and amorphous solids usually result. In the formation of amorphous citrate solids, since no driving force for aggregation arises among constituents, a precursor mixture which reflects the homogeneity in the solution can be obtained. In the silica gel, the formation of nickel citrate also suppresses the aggregation of nickel species by crystallization during drying. Since the distribution of nickel citrate in the dried silica gel probably reflects homogeneity in the wet gel, the NiO particles formed by the decomposition of nickel citrate are distributed homogeneously in the silica matrix after heating, as observed in the TEM micrographs (Figs. 5 and 6). In addition, growth of NiO is also effectively suppressed, and small NiO particles with sizes of ~6.5 nm result because the pore structure of the silica gel becomes rigid after being dried at 50°C.

Furthermore, the particle size of NiO as well as Ni metal can be decreased by heating in N_2 flow. In the air, the nickel citrate exothermically decomposed into nickel oxide. Then, the formed nickel oxide grows until the particle size becomes the same size as the pores because of a local heating effect caused by the burning of citrate. In contrast, heating under an N_2 flow allows milder decomposition of the nickel citrate, not to proceed the growth of nickel oxide. In addition, residual carbons in the nickel oxides probably affect the crystallization of them and their growth, leading to the formation of crystallites with many defects. These defects could enhance the reduction of nickel oxide crystallites at low temperatures, as observed in the TPR profile (Fig. 4a).

Catalytic Activities of Ni/SiO_2 for Hydrogenation of Benzene

In the present work, we can prepare Ni/SiO_2 catalysts with different NiO particle sizes, 9 (NA–air), 6.5 (CA–air), and 3.5 nm (CA–N_2), irrespective of a NiO content of up to 26 mol%, by adopting the solution exchange method using citric acid additives. From the structural feature of the silica gel together with the nature of nickel nitrate and nickel citrate, we have proposed a mechanism for how particle size

is controlled. The present results indicate that inhibition of the aggregation of Ni species in drying is important in increasing Ni dispersion rather than bond formation between Si and Ni in the wet gel.

The Ni surface area is almost proportional to Ni loading for each series of samples (Table 1), and the catalytic activity increases with an increasing amount of surface Ni at 80°C (Fig. 12). In addition, TOF increases with a decrease in particle size (Fig. 13). Although the hydrogenation of benzene is classified as structure insensitive, size dependence of TOF has been reported for Ni/SiO_2 (56). The present results essentially agree with the data in the literature (56). The deviation in some data points in Fig. 13 is probably attributable to other structural effects, such as pore size, pore volume, and exposure degree of Ni particles. Thus, the hydrogenation activity of Ni/SiO_2 can be effectively increased by decreasing Ni particle size through an increase in both the amount of surface Ni and TOF.

CONCLUSION

A Ni/SiO_2 catalyst is prepared by solution exchange method, where the Ni is supported on silica by exchanging the solution in wet silica gel with a Ni-containing solution. The Ni/SiO_2 prepared by the solution exchange with an aqueous 1 mol dm^{-3} nitric acid solution has mesopores ca. 4 nm in size and with a relatively large BET surface area. The distribution of NiO and Ni particles in the gel matrix as well as their size can be controlled by adding citric acid to the exchange solution and by heating in an N_2 flow.

When an aqueous nickel nitrate solution is used in solution exchange, nickel nitrate crystallizes within the gel matrix during drying. The decomposition of nickel nitrate into small NiO particles in heating produces a characteristic distribution of NiO particles in the gel matrix. On the other hand, the use of citric acid together with nickel nitrate in solution exchange effectively inhibits the aggregation of Ni species in drying by forming nickel citrate, which barely crystalizes in drying. In heating, the nickel citrates decompose into NiO particles, while their distribution in the silica matrix becomes homogeneous. The growth of NiO particles can be suppressed by calcination under an N_2 flow. Thus, we can prepare a Ni/SiO_2 catalyst with a small Ni particle size and high Ni surface area even at high Ni content, which shows superior catalytic activity for the hydrogenation of benzene.

ACKNOWLEDGMENTS

The authors thank Prof. Katsuyuki Ogura, Chiba University, for the use of NMR apparatus, and Prof. Kazuki Nakanishi, Kyoto University, for the use of SAXS apparatus. Financial support from Grant-in-Aid for Encouragement of Young Scientists (11750580) and Grant-in Aid for Scientific Research C (12650075) is gratefully acknowledged.

REFERENCES

1. Morikawa, K., Shirasaki, T., and Okawa, M., *Adv. Catal.* **20**, 97 (1969).
2. Vannice, A. M., *Catal. Rev. —Sci. Eng.* **14**, 153 (1976).
3. Ruckenstein, E., and Hu, Y. H., *J. Catal.* **162**, 230 (1996).
4. Keane, M. A., *J. Catal.* **166**, 347 (1997).
5. Klvana, D., Chaouki, J., Kusohorosky, D., Chavarie, C., and Pajonk, G., *Appl. Catal.* **42**, 121 (1998).
6. Gamman, J. J., Millar, G. J., Rose, G., and Drennan, J., *J. Chem. Soc. Faraday Trans.* **94**, 701 (1998).
7. Kim, J., Suh, D. J., Park, T. J., and Kim, K., *Appl. Catal. A* **197**, 191 (2000).
8. Brinker, C. J., and Scherer, G. W., *in* "Sol–Gel Science. The Chemistry and Physics of Sol–Gel Processing." Academic Press, New York, 1990.
9. Cauqui, M. A., and Rodriguez-Izquierdo, J. M., *J. Non-Cryst. Solids* **147/148**, 724 (1992).
10. Toba, M., Mizukami, F., Niwa, S., and Maeda, K., *J. Chem. Soc. Chem. Commun.* 1211 (1990).
11. Miller, J., Rankin, S., and Ko, E., *J. Catal.* **148**, 673 (1994).
12. Miller, J., and Ko, E., *J. Catal.* **159**, 83 (1996).
13. Ueno, A., Suzuki, H., and Kotera, Y., *J. Chem. Soc., Faraday Trans.* **79**, 127 (1983).
14. Tohji, K., Udagawa, Y., Tanabe, S., and Ueno, A., *J. Am. Chem. Soc.* **106**, 612 (1984).
15. Niwa, S., Mizukami, F., Isoyama, S., Tsuchiya, T., Shimizu, K., Imai, S., and Imamura, J., *J. Chem. Tech. Biotechnol.* **36**, 236 (1986).
16. Breitscheidel, B., Zieder, J., and Schubert, U., *Chem. Mater.* **3**, 559 (1991).
17. Lopez, T., Bosch, P., Asomoza, M., and Gomez, R., *J. Catal.* **133**, 247 (1992).
18. Zou, W., and Gonzalez, R., *J. Catal.* **152**, 291 (1995).
19. Takahashi, R., Nakanishi, K., and Soga, N., *J. Non-Cryst. Solids* **189**, 66 (1995).
20. Takahashi, R., Nakanishi, K., and Soga, N., *Faraday Discuss.* **101**, 249 (1995).
21. Takahashi, R., Sato, S., Sodesawa, T., Kato, M., and Yoshii, T., *Chem. Lett.* 305 (1999).
22. Takahashi, R., Sato, S., Sodesawa, T., Suzuki, M., and Ogura, K., *Bull. Chem. Soc. Jpn.* **73**, 765 (2000).
23. Takahashi, R., Nakanishi, K., and Soga, N., *J. Sol–Gel Sci. Technol.* **17**, 7 (2000).
24. Dollimore, D., and Heal, G. R., *J. Appl. Chem.* **14**, 109 (1964).
25. Bartholomew, C. H., and Farrauto, R. J., *J. Catal.* **45**, 41 (1976).
26. Sato, S., Takahashi, R., Sodesawa, T., Nozaki, F., Jin, X. Z., Suzuki, S., and Nakayama, T., *J. Catal.* **191**, 261 (2000).
27. Yasumori, A., Anma, M., and Yamane, M., *Phys. Chem. Glasses* **30**, 193 (1989).
28. Mile, B., Stirling, D., Zammitt, M. A., Lovell, A., and Webb, M., *J. Catal.* **114**, 217 (1998).
29. Takahashi, R., Sato, S., Sodesawa, T., Kato, M., and Yoshida, S., *J. Sol–Gel Sci. Technol.* **19**, 715 (2000).
30. Burattin, P., Che, M., and Louis, C., *J. Phys. Chem. B* **101**, 7060 (1997).
31. Burattin, P., Che, M., and Louis, C., *J. Phys. Chem. B* **102**, 2722 (1998).
32. Takahashi, R., Sato, S., Sodesawa, T., and Kamomae, Y., *Phys. Chem. Chem. Phys.* **2**, 1199 (2000).
33. Brinker, C. J., Keefer, K. D., Schaefer, D. W., Assink, R. A., Kay, B. D., and Asheley, C. S., *J. Non-Cryst. Solids* **63**, 45 (1984).
34. Brinker, C. J., and Scherer, G. W., *J. Non-Cryst. Solids* **75**, 301 (1985).
35. Tanaka, T., Ishiwata, S., and Ishimoto, C., *Phys. Rev. Lett.* **38**, 771 (1977).
36. Tanaka, T., *Phys. Rev. Lett.* **40**, 820 (1978).
37. Iler, R. K., *in* "The Chemistry of Silica." Wiley, New York, 1979.
38. Quinson, J. F., Tchipkam, N., Dumas, J., Bovior, C., Serughetti, J., Guizard, C., Larbot, A., and Cot, L., *J. Non-Cryst. Solids* **99**, 151 (1988).

39. Quinson, J. F., Dumas, J., Chatelut, M., Serughetti, J., Guizard, C., Larbot, A., and Cot, L., *J. Non-Cryst. Solids* **113**, 14 (1989).
40. Nakanishi, K., Sagawa, Y., and N. Soga, *J. Non-Cryst. Solids* **134**, 39 (1991).
41. Davis, P. J., Brinker, C. J., and Smith, D. M., *J. Non-Cryst. Solids* **142**, 189 (1992).
42. Davis, P. J., Brinker, C. J., Smith, D. M., and Assink, R. A., *J. Non-Cryst. Solids* **142**, 197 (1992).
43. Nakanishi, K., Takahashi, R., and Soga, N., *J. Non-Cryst. Solids* **147/148**, 291 (1992).
44. Marcilly, C., Courty, P., and Delmon, B., *J. Am. Ceram. Soc.* **53**, 56 (1970).
45. Courty, P., Ajot, H., Marcilly, C., and Delmon, B., *Powder Technol.* **7**, 21 (1973).
46. Baythoun, M. S. G., and Sale, F. R., *J. Mater. Sci.* **17**, 2757 (1982).
47. Patrick, V., and Gavalas, G., *J. Am. Ceram. Soc.* **73**, 358 (1990).
48. Sato, S., Nozaki, F., and Nakayama, T., *Appl. Catal. A* **139**, L1 (1996).
49. Nakayama, T., Ichikuni, N., Sato, S., and Nozaki, F., *Appl. Catal. A* **158**, 185 (1997) .
50. Sato, S., Takahashi, R., Sodesawa, T., Yuma, K., and Obata, Y., *J. Catal.* **196**, 195 (2000).
51. Sato, S., Iijima, M., Nakayama, T., Sodesawa, T., and Nozaki, F., *J. Catal.* **169**, 447 (1997).
52. Sato, S., Koizumi, K., and Nozaki, F., *J. Catal.* **178**, 264 (1998).
53. Sato, S., Takahashi, R., Sodesawa, T., Matsumoto, K., and Kamimura Y., *J. Catal.* **184**, 180 (1999).
54. Kamimura, Y., Sato, S., Takahashi, R., Sodesawa, T., and Fukui, M., *Chem. Lett.* 232 (2000).
55. Lopez-Quintela, M. A., Knoche, W., and Veith, J., *J. Chem. Soc., Faraday Trans. 1* **80**, 2313 (1984).
56. Che, M., and Bennett, C. O., *Adv. Catal.* **36**, 55 (1989).